NANO LETTERS

pubs.acs.org/NanoLett Letter

Sub-5 nm Anisotropic Pattern Transfer via Colloidal Lithography of a Self-Assembled GdF_3 Nanocrystal Monolayer

Austin W. Keller, Emanuele Marino, Di An, Steven J. Neuhaus, Katherine C. Elbert, Christopher B. Murray,* and Cherie R. Kagan*

Cite This: *Nano Lett.* 2022, 22, 1992–2000 Read Online

ACCESS | Metrics & More | Article Recommendations | Supporting Information

ABSTRACT: Patterning materials with nanoscale features opens many research opportunities ranging from fundamental science to technological applications. However, current nanofabrication methods are ill-suited for sub-5 nm patterning and pattern transfer. We demonstrate the use of colloidal lithography to transfer an anisotropic pattern of discrete features into substrates with a critical dimension below 5 nm. The assembly of monodisperse, anisotropic nanocrystals (NCs) with a rhombic-plate morphology spaced by dendrimer ligands results in a well-ordered monolayer that serves as a 2D anisotropic hard mask pattern. This pattern is transferred into the underlying substrate using dry etching followed by removal of the NC mask. We exemplify this approach by fabricating an array of pillars with a rhombic cross-section and edge-to-edge spacing of 4.4 ± 1.1 nm. The fabrication approach enables broader access to patterning materials at the deep nanoscale by implementing innovative processes into well-established fabrication methods while minimizing process complexity.

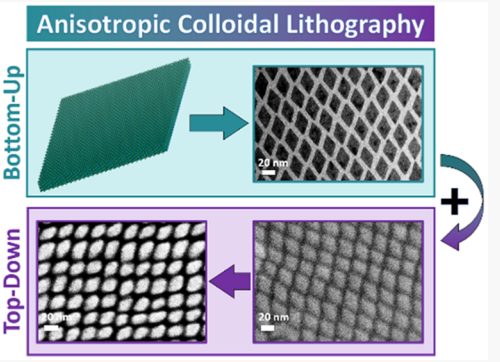

KEYWORDS: *sub-5 nm fabrication, anisotropic pattern transfer, colloidal lithography, nanolithography, nanocrystal self-assembly*

The semiconductor industry has been the most significant driving force for developing nanoscale technology. Since its inception, this industry has relied heavily on photolithography to achieve high-throughput patterning over large areas. Although challenging, the frontier of nanofabrication capabilities has pushed conventional photolithography to sub-20 nm patterning using various resolution enhancement techniques. The development of extreme ultraviolet (EUV) tooling has recently led to the commercialization of EUV lithography for state-of-the-art patterning below 10 nm,[1−3] where it is used to define the three-dimensional channel, known as a fin, of field-effect transistors (FETs or finFETs). Ongoing efforts aim to realize patterning below 5 nm to extend Moore's law for integrated circuit technology and memory devices. The ability to fabricate features or their spacings below 5 nm would also advance research for the development of metasurfaces,[4,5] optoelectronic devices,[6] and quantum technologies.[7−9]

However, it is unclear whether EUV lithography can reliably pattern features below 5 nm,[10,11] and the extremely high cost of EUV systems is prohibitive for research purposes that require prototyping or for small-volume production markets. Thus, researchers have developed several other specialized fabrication methods for patterning at small length scales, including direct-write methods like focused ion beam lithography,[12−15] electron beam lithography,[16−18] and scanning probe lithography[19−21] and other approaches such as nanoimprint lithography[22−24] and post-trimming methods.[25,26] Each technique has strengths and limitations. For example, direct-write methods offer precision and arbitrary pattern design but generally suffer from low throughput.[27] Nanoimprint lithography provides high throughput[24] but generally does not offer as high resolution or precision in overlay registration as direct-write methods. These top-down lithographic approaches typically yield features larger than 10 nm. Efforts toward sub-10 nm patterning have been limited by low feature density,[14,16,19,28−31] and the few efforts that have achieved sub-5 nm pattern transfer have demonstrated relatively isolated features or have been limited to 1D patterns.[16,32−34]

In contrast to purely top-down approaches, self-assembly methods such as directed self-assembly (DSA) of block copolymers and colloidal lithography have been widely implemented to integrate bottom-up patterning with top-down pattern transfer. Block copolymer DSA leverages nanoscale phase segregation, where one phase is then selectively removed to form a mask of various pattern

Received: December 9, 2021
Revised: February 18, 2022
Published: February 28, 2022

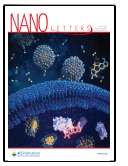

https://doi.org/10.1021/acs.nanolett.1c04761
Nano Lett. 2022, 22, 1992−2000

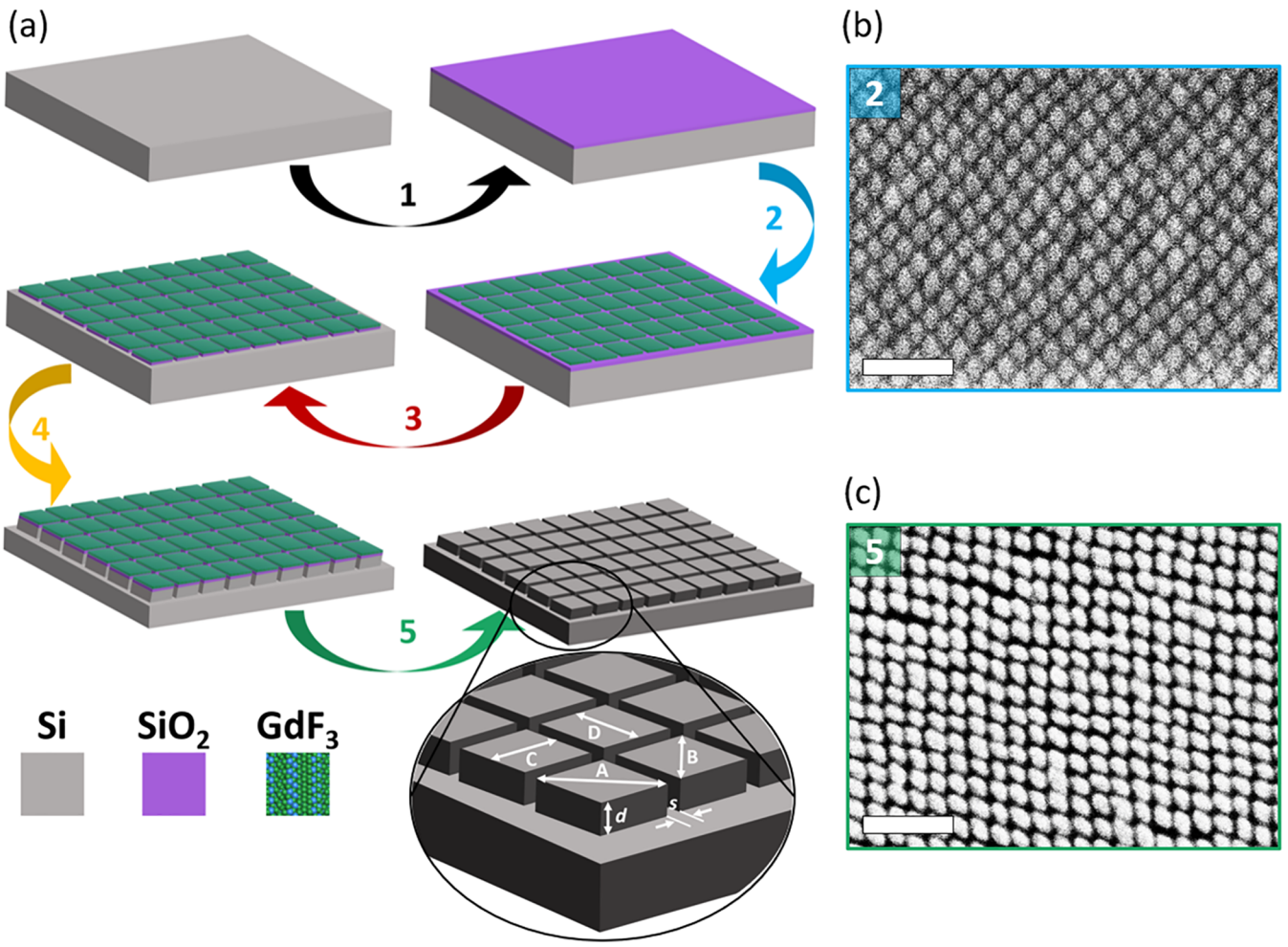

Figure 1. (a) Schematic overview of the anisotropic pattern transfer process. [1] A ∼7 nm film of SiO_2 is grown on a Si wafer using a dry thermal oxidation process and is functionalized with a silane molecule to make the surface hydrophobic. [2] The NC monolayer assembly is transferred from a liquid−air interface to the substrate surface. [3] An O_2 descum process is used to remove the ligands and any residual organic material; then the thin SiO_2 layer is etched in regions between the NCs using a short CF_4/O_2 ICP RIE. [4] The underlying Si substrate is then etched using Cl_2/Ar ICP RIE to transfer the anisotropic pattern. [5] The NC mask layer is removed via liftoff of the underlying SiO_2 layer using a 10% HF wet etch. The magnified view of the patterned substrate shows lateral dimensions *A*, *B*, *C*, and *D*, which are set by the NC mask size, spacing *s*, which is set by the interparticle spacing of the NC assembly, and etch depth *d*, which is determined by the dry etch conditions. (b) SEM image of the GdF_3-D NC monolayer assembly on a SiO_2/Si substrate (step 2). (c) SEM image of the patterned Si substrate after NC mask and SiO_2 removal (step 5). Scale bars are 100 nm.

morphologies.[35−37] Most pattern transfer demonstrations using this approach, including 2D morphologies like hexagonal or square motifs, have exhibited a critical dimension greater than 20 nm. Efforts toward smaller feature sizes have only been realized in 1D patterns.[38−42] Importantly, controlled morphology with high resolution resulting from block copolymer DSA typically requires predefined topographic[39,40,43,44] or chemical[45−47] patterning, increasing the process complexity. A major drawback for pattern transfer with this approach is that polymer structures generally suffer from low etch selectivity and require sequential infiltration synthesis to enhance etch resistance[48−50] or the use of a secondary hard mask.[41]

Colloidal lithography offers a different approach by using particles as building blocks that are assembled to establish a pattern, where each particle serves as a discrete mask for subsequent deposition or etching.[51−53] Most demonstrations of pattern transfer using colloidal lithography have fabricated features larger than 50 nm.[54−58] The few examples that have explored the sub-50 nm regime have utilized close-packed spherical NCs, leading to isotropic features with hexagonal ordering.[59−61] There has yet to be a high-fidelity pattern transfer demonstration of discrete anisotropic features below 40 nm. Here, we demonstrate 2D patterning and subsequent pattern transfer of high-density anisotropic features with a critical dimension below 5 nm via NC colloidal lithography, which can be performed in a standard fabrication facility. Our approach integrates bottom-up NC synthesis and self-assembly with top-down dry etching to realize high-fidelity pattern transfer into the desired substrate.

The bottom-up patterning approach employs monodisperse anisotropic GdF_3 NCs as exemplary building blocks. The NCs have a faceted rhombic-plate morphology and the GdF_3 imparts high etch selectivity for both fluorine- and chlorine-based dry etch chemistries. The NCs are functionalized with a dendrimer ligand that provides colloidal stability and defines the spacing between the NCs upon assembly,[62] similar to the concept of molecular rulers.[63] The anisotropic pattern is realized by assembling the NCs at the liquid−air interface[64−67]

https://doi.org/10.1021/acs.nanolett.1c04761
Nano Lett. 2022, 22, 1992−2000

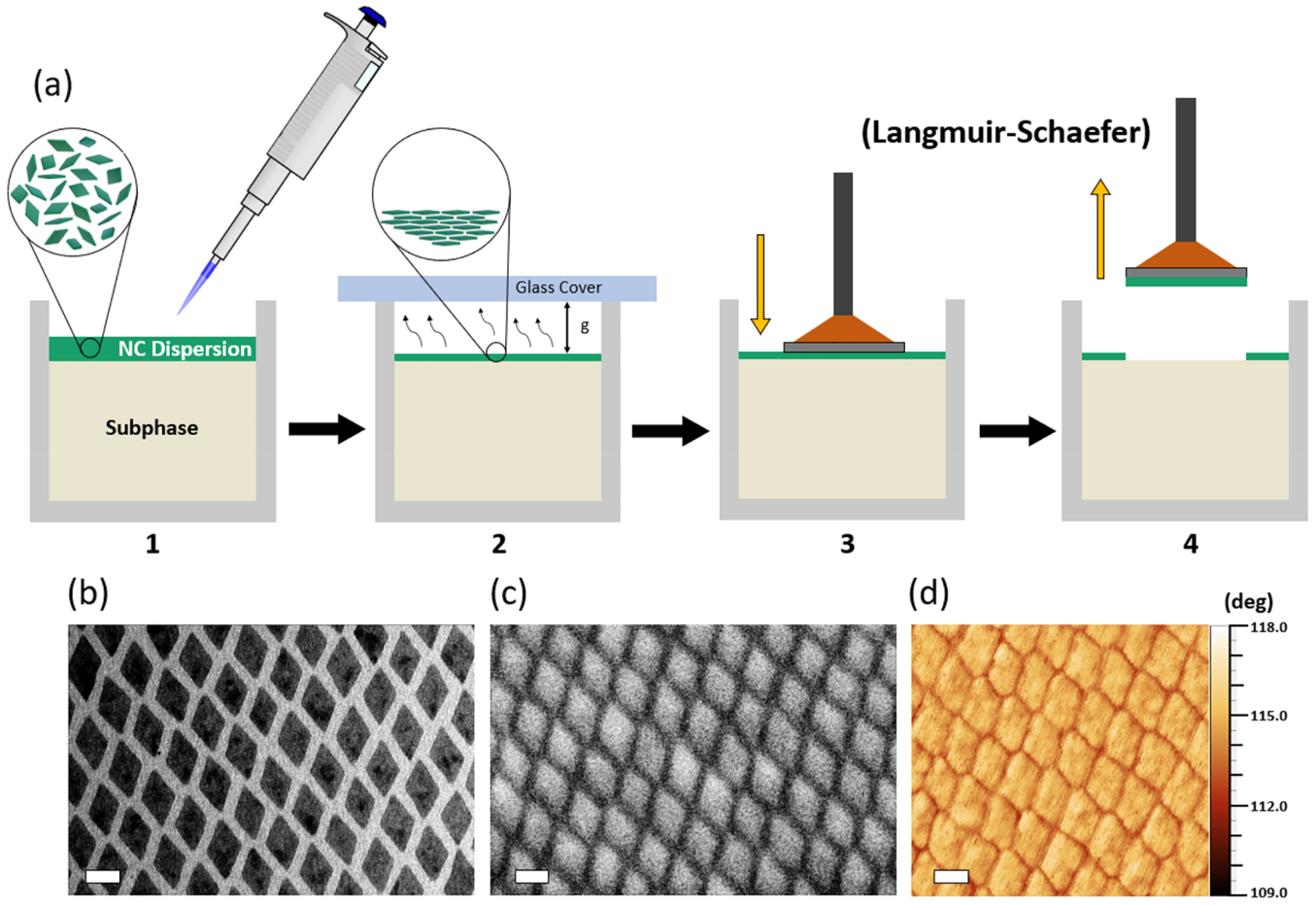

Figure 2. (a) Cross-sectional schematic of the liquid−air interfacial self-assembly technique and subsequent film transfer onto a substrate via the Langmuir−Schaefer method. [1] The desired volume of the NC dispersion is drop-cast onto the liquid subphase. [2] The well is covered with a glass slide to decrease the evaporation rate and allow the self-assembly process to occur. [3] The glass slide is removed when the NC film is completely dry; then the substrate surface is carefully lowered toward the NC film until contact is made. [4] The substrate is translated vertically upward, any excess subphase is wicked away, and the sample is dried under vacuum. (b) TEM, (c) SEM, and (d) AFM (phase contrast) images of a well-ordered monolayer assembly of GdF_3-D NCs on a substrate using the assembly method described in panel a. Scale bars are 20 nm.

into a well-ordered monolayer, where each NC serves as a discrete etch mask. This pattern is then transferred into the underlying substrate using inductively coupled plasma (ICP) reactive ion etching (RIE), after which the NC mask layer is selectively removed to realize a 2D patterned substrate surface of rhombic pillars (32 nm × 21 nm) with a sub-5 nm spacing set by the dendrimer ligand. To date, the authors are not aware of any work that has been able to simultaneously combine the three aspects for pattern transfer that we successfully demonstrate: (1) a sub-5 nm critical dimension, (2) a 2D pattern with high feature density, and (3) discrete anisotropic features.

A schematic overview of the fabrication process is shown in Figure 1a. Using a mild, dry thermal oxidation process, we grow a 7 nm SiO_2 layer on a Si substrate and perform a silanization treatment to make the surface hydrophobic (step 1). A well-ordered monolayer of monodisperse anisotropic rhombic-plate NCs is formed via self-assembly at the liquid−air interface. This ordered NC monolayer is transferred to the substrate surface using the Langmuir−Schaefer method (step 2), as shown by the representative SEM image in Figure 1b. After a brief O_2 plasma descum process, we use ICP RIE with CF_4/O_2 chemistry to etch through the thin SiO_2 layer (step 3) and then etch into the underlying Si substrate using Cl_2/Ar ICP RIE (step 4). We finally remove the NC monolayer by a wet etch liftoff of the underlying SiO_2 layer using hydrofluoric acid (step 5), leaving behind the patterned Si substrate, as shown in Figure 1c. The thin SiO_2 film serves as a sacrificial liftoff layer for NC mask removal and can act as a secondary etch mask when using Cl_2-based chemistry. Figure S1 depicts a schematic cross-sectional view of this pattern transfer process. The magnified view in Figure 1a shows the patterned features with long axis *A* and shorter axis *B*, widths *C* and *D* between the parallel sides, edge-to-edge spacing *s*, and pillar height *d*.

We synthesize monodisperse GdF_3 rhombic plates doped with Er^{3+} and Yb^{3+} and functionalized with oleate ligands (GdF_3−OA) to serve as building blocks. The plate thickness (*t*) is 2.2 nm. There are four characteristic lateral dimensions. The diagonal axis dimensions *A* and *B* are 37.3 ± 1.9 nm and 22.6 ± 1.2 nm, respectively. The dimensions normal to the parallel sides, *C* and *D*, are 20.5 ± 1.2 nm and 22.6 ± 1.2 nm, respectively. Figure S2 provides a detailed characterization of the anisotropic GdF_3 NC morphology. We replace native oleates with a bulkier dendrimer ligand (GdF_3-D) through a solution-based ligand exchange procedure.[67] The dendrimer provides improved colloidal stability to prevent NCs from stacking in solution (described by Figure S3) to yield NC

https://doi.org/10.1021/acs.nanolett.1c04761
Nano Lett. 2022, 22, 1992−2000

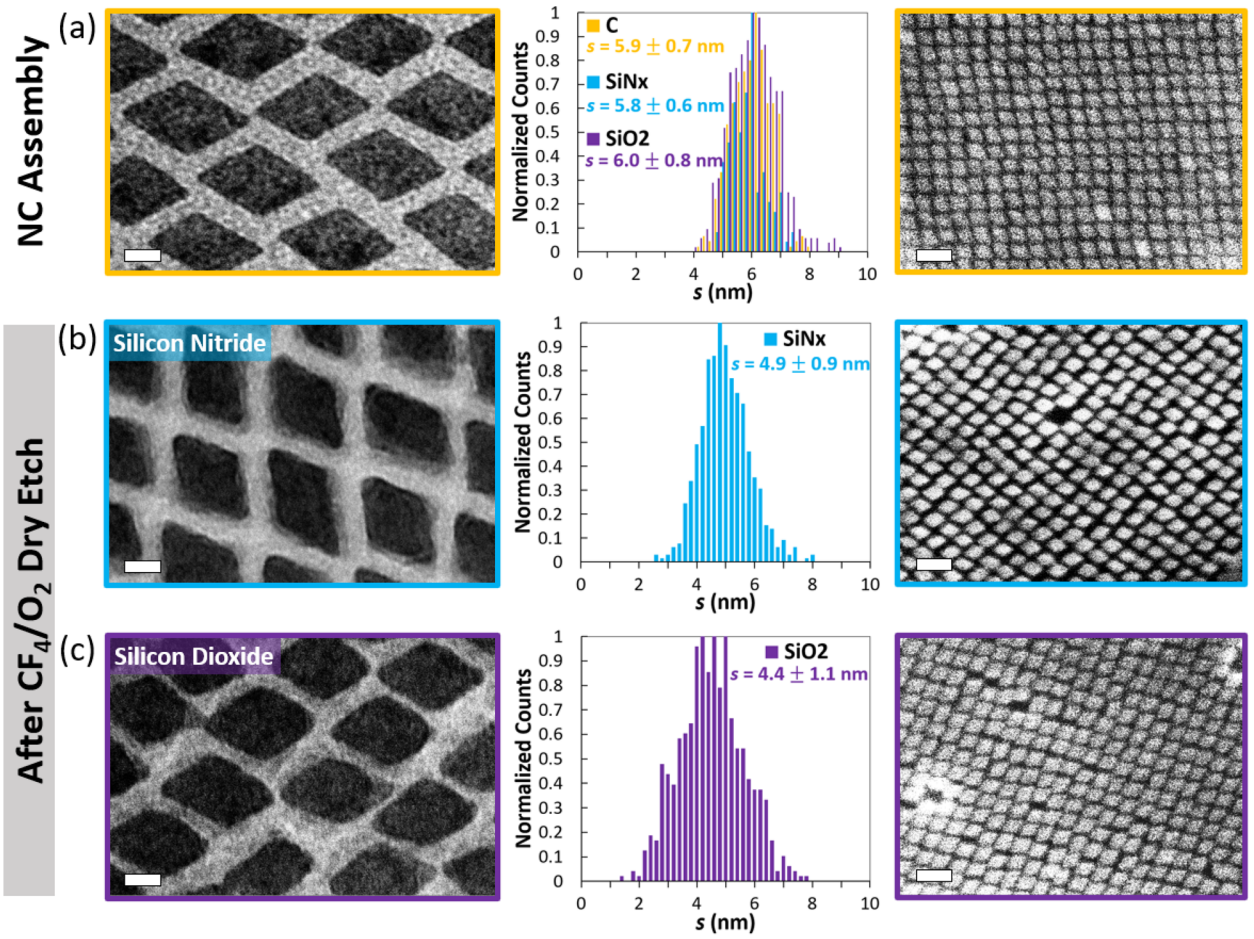

Figure 3. Characterization of pattern transfer and the critical dimension s using 2D assemblies of discrete, anisotropic GdF_3-D NC masks. (a) Characterization of GdF_3-D monolayer assembly. The histogram shows consistency in s regardless of substrate material. (b, c) Characterization of pattern transfer into (b) SiN_x and (c) SiO_2 via ICP RIE. (left) Representative TEM image. (middle) Histogram of edge-to-edge spacing s using measurements from TEM characterization of 500 interparticle spacings. (right) Representative SEM image. The GdF_3 NCs are still present in panels b and c after the dry etch process. The SEM images in panels b and c show pattern transfer into the respective bulk substrate. Scale bars are 10 nm for the TEM images and 50 nm for the SEM images.

assemblies with improved order, and the dendrimer sets the interparticle spacing.

A prerequisite for high-quality pattern transfer is the organization of highly ordered NC assemblies. We achieve this ordering through self-assembly at the liquid−air interface, as shown in Figure 2a. The self-assembly process begins with filling a 2.25 × 2.25 × 1.5 cm^3 Teflon well with 3.2 mL of ethylene glycol (EG). The GdF_3-D NC dispersion in toluene is then drop-cast onto the EG surface using 80 μL at a 0.2 mg/mL concentration. The well is quickly covered with a glass slide to decrease the solvent evaporation rate and allow the self-assembly process to occur. After solvent evaporation, the glass slide is removed, and the substrate is carefully lowered face-down to the surface of the liquid subphase until contact is made. The substrate is lifted vertically, any excess liquid subphase is removed by wicking with a clean wipe, and the sample is dried under vacuum at 50 °C. The backside of the substrate is held by a suction device to keep the substrate surface parallel to the liquid−air interface. Environmental conditions such as temperature and humidity affect the solvent evaporation rate and therefore influence the assembly process. Faster drying typically results in multilayer films and can lead to poor film uniformity and degraded local order. We perform NC assembly in an air-filled glovebox, which controls relative humidity to tune the dew point to ∼10 °C. Full process details can be found in the Supporting Information.

Representative TEM, SEM, and AFM images of the resulting anisotropic NC mask pattern prepared by self-assembly are shown in Figure 2b−d, respectively. The NCs are assembled parallel to the substrate with commensurate ordering of the facets. The anisotropic NC pattern exhibits uniformity in feature size, shape, orientation, and spacing due to the narrow dispersity of the GdF_3-D NCs. The self-assembly process naturally results in ordered NC grains separated by grain boundaries. The anisotropic NCs are oriented in the same direction within a grain, but the orientation varies between different grains across the substrate. Figure S4 shows typical grain sizes, which have an edge length of approximately 1−2 μm. Within an ordered domain, the edge-to-edge spacing (s) between the NCs is set by the organic ligand shell. We will consider s to be the critical dimension (CD) of the pattern since the space between the inorganic NC masks will be etched during pattern transfer.

Figure 3 provides an analysis of s before and after pattern transfer. The left column of Figure 3 shows a representative TEM image with a corresponding histogram of the edge-to-edge spacing s in the middle column, and a representative SEM image in the right column. While TEM offers higher resolution

https://doi.org/10.1021/acs.nanolett.1c04761
Nano Lett. 2022, 22, 1992−2000

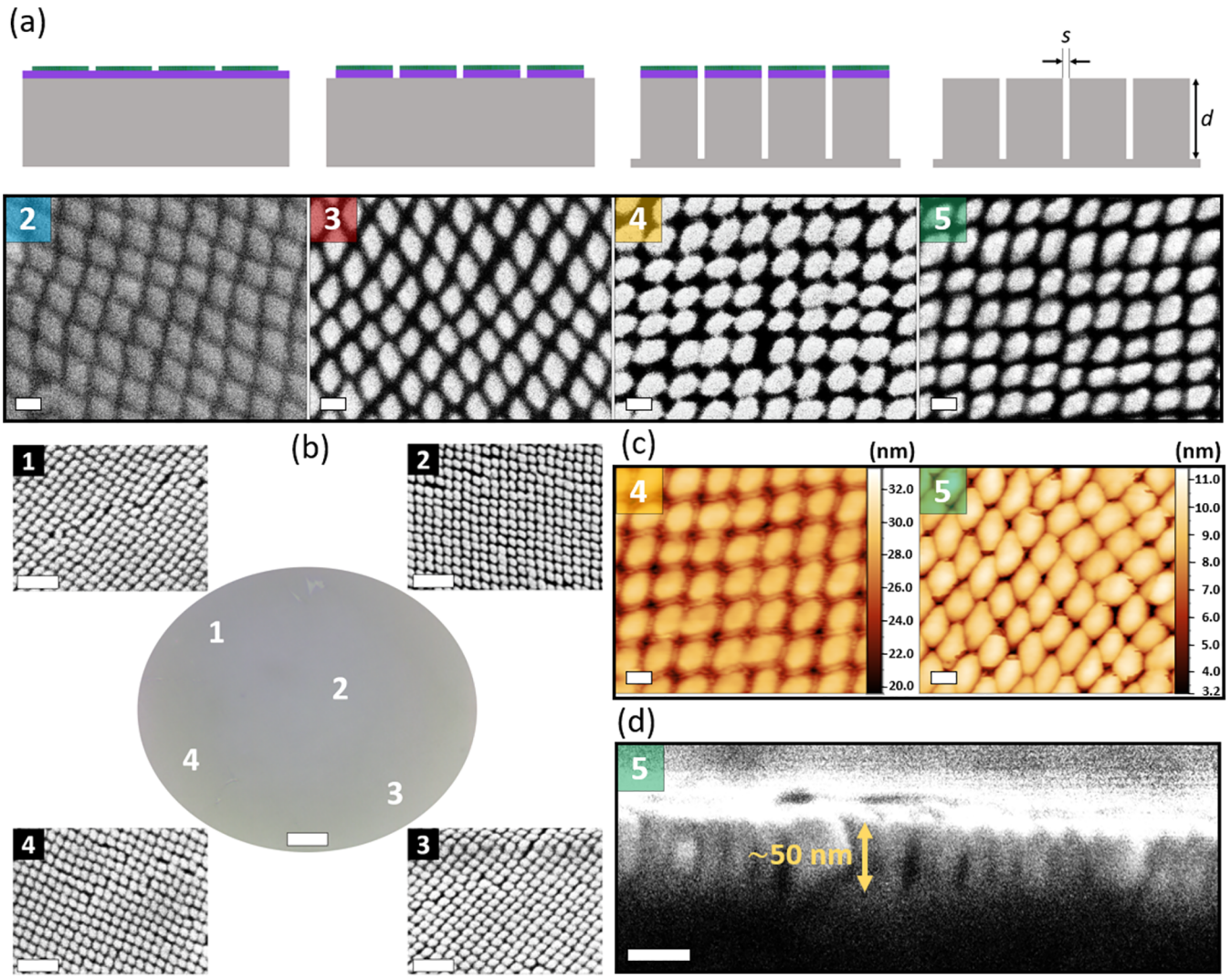

Figure 4. Characterization of the complete pattern transfer process on bulk Si as described in Figure 1. (a) Schematic cross sections and corresponding top-down SEM images after process steps 2−5. Step 5 is post-NC liftoff, leaving behind only the patterned Si substrate. Scale bars are 20 nm. (b) Characterization after mask removal (step 5) over a large area. Bright-field optical image of the sample surface (center). The surrounding SEM images correspond to locations 1−4 indicated on the optical image. The scale bar is 10 μm in the optical image and 100 nm in the SEM images. (c) AFM height characterization of the patterned surface after steps 4 and 5. Scale bars are 20 nm. (d) Cross-sectional SEM image of the patterned Si surface after mask removal showing the feature height $d \approx 50$ nm. The scale bar is 50 nm.

over both SEM and AFM, the low penetration depth of the electrons inherently makes top-down characterization on a bulk substrate infeasible. To enable higher-resolution characterization using TEM, we perform the patterning and pattern transfer steps on thin membranes of SiN_x and SiO_2, two commonly used materials in device fabrication. Figure 3a shows characterization of the assembled NC mask pattern. As demonstrated by testing on carbon, SiN_x, and SiO_2 membranes, transferring the NC pattern to a different substrate material does not affect the spacing s. The dendrimer ligand yields a CD of $s = 5.9 \pm 0.7$ nm, $s = 5.8 \pm 0.6$ nm, and $s = 6.0 \pm 0.8$ nm for the carbon, SiN_x, and SiO_2 membrane, respectively.

After patterning the substrate surface with the assembled NC mask, we perform pattern transfer onto the SiN_x and SiO_2 substrates via ICP RIE using CF_4-based etch chemistry and analyze s after pattern transfer, as shown in Figure 3b,c. TEM characterization and analysis of the feature spacing post-etching show a decrease in s of 0.9 nm for SiN_x and 1.6 nm for SiO_2, placing the mean CD as 4.9 ± 0.9 nm and 4.4 ± 1.1 nm for SiN_x and SiO_2, respectively. This decrease in s is most likely a consequence of the dry etch process. The CF_4-based etch chemistry is an inhibitor-driven process that enables vertical etch anisotropy due to the formation of a fluorocarbon passivation layer on all surfaces.[68,69] The areas normal to the incident direction of ions and radicals are etched more efficiently than the passivated sidewalls, enabling the formation of a relatively vertical etch profile. The formation of the thin passivation layer on the channel sidewalls likely contributes to the observed decrease in s. A decrease of 1.0 nm in s means there is only a 0.5 nm broadening on either side of the channel, indicating a precise pattern transfer result that exhibits high fidelity to the original NC mask. Figure S5 provides a more detailed summary of the feature dimensions before and after dry etching for the SiO_2 membrane. We specifically focus our analysis on SiO_2 since we employ a thin film of SiO_2 for the complete pattern transfer process into a bulk Si substrate. The resulting pattern transfer morphology in the SiO_2 layer directly

https://doi.org/10.1021/acs.nanolett.1c04761
Nano Lett. 2022, 22, 1992−2000

influences the subsequent pattern transfer to the Si. Analysis of TEM data for the SiO_2 membrane reveals that the sharp corners are rounded after the etch process, resulting in a decrease in the mean of dimensions *A* and *B* by 5.1 and 1.7 nm, respectively. The mean of dimensions *C* and *D* increased by 1.0 and 1.1 nm, respectively.

The SEM images in the right panel of Figure 3b,c show the pattern transfer result performed on bulk SiN_x and SiO_2, demonstrating high-quality pattern transfer over a length scale of hundreds of nanometers with a high feature density. The linear feature density is defined as FD = a/p, where a is the feature size and p is the feature pitch. One-dimensional line-space patterns have been fabricated with FD > 0.5 for larger features, but not for sub-5 nm features. Most demonstrations of sub-5 nm pattern transfer have only realized isolated features or demonstrated FD < 0.1.[27,70] If we consider the critical dimension s as the feature size a, the channel feature density in directions *C* and *D* are ∼0.17 and ∼0.16, respectively, for the SiO_2 substrate. A more detailed description of the feature pitch is provided by Figure S6. The corresponding feature density of the rhombic pillars in directions *C* and *D* are ∼0.83 and ∼0.84, respectively, for the SiO_2 substrate.

Returning to fabrication on a bulk SiO_2/Si substrate, we note that the hydrophilic nature of SiO_2 poses issues with film transfer of the hydrophobic NC assembly from the liquid−air interface to the substrate surface. To promote successful film transfer and improve the adhesion of the NC monolayer to the SiO_2/Si substrate, we functionalize the SiO_2 surface with a hydrophobic silane (e.g., methyltrimethoxysilane), as described by Figure S7. We note that the complete process flow is compatible with the use of several other silanes at this step, as demonstrated in Figure S8. The complete patterning and pattern transfer process for anisotropic features with a critical dimension below 5 nm on a bulk SiO_2/Si substrate is demonstrated in Figure 4a, where the numbers and corresponding cross-sectional schematics refer to the steps described in Figure 1a. After the NC film is transferred to the substrate, the ligands are removed through an O_2 descum process. The anisotropic pattern set by well-ordered NC assembly (step 2) is first transferred to the SiO_2 layer using CF_4/O_2 chemistry (step 3), then to the bulk Si substrate using Cl_2/Ar chemistry (step 4), followed by NC mask liftoff (step 5). The specific dry-etch chemistry and process conditions determine the final feature height, *d*. Full process details can be found in the Supporting Information.

To confirm the efficacy of our liftoff process in step 5, we collect upconversion photoluminescence spectra before and after liftoff, as shown in Figure S9. Before liftoff, we observe peaks around 545 nm and 655 nm, which are characteristic of the Yb^{3+}- and Er^{3+}-doped GdF_3 NCs.[66,71,72] These peaks are no longer detectable post-liftoff, confirming the successful removal of the NCs. Figure 4b shows characterization of the cleanly patterned Si substrate surface after mask liftoff. The central bright-field optical image highlights the uniformity of the substrate surface, which is patterned across a centimeter length scale. The surrounding SEM images in Figure 4b correspond to the locations 1−4 indicated on the optical image.

To characterize the patterned surface beyond top-down SEM images, Figure 4c shows AFM height data, which reveal the surface topography after process steps 4 and 5. Figure S10 provides an AFM line scan measurement after NC mask removal. While AFM provides high-resolution height measurements and the visualization of the sample topography, the sample morphology makes it inherently challenging to analyze the true pillar height. Since the feature spacing is less than 5 nm, even the sharpest AFM probes available cannot reach the bottom of the etched channels, highlighting the success of our approach for pattern transfer at the deep nanoscale. For a clearer view, Figure 4d provides a cross-sectional SEM image after mask removal (step 5), which reveals $d \approx 50$ nm. The resulting feature height is sensitive to process conditions and could be increased or decreased by adjusting the Cl_2/Ar ICP RIE conditions such as etch time and high frequency (HF) power.

In summary, we demonstrate pattern transfer of anisotropic features to substrates with a critical dimension below 5 nm by integrating bottom-up and top-down strategies. A self-assembled, well-ordered monolayer of monodisperse GdF_3 NCs with an anisotropic rhombic-plate morphology functionalized with dendrimer ligands sets the anisotropic hard mask pattern on a desired substrate material. This pattern is transferred into the underlying substrate using conventional dry etching with ICP RIE, followed by selective removal of the NC mask. To the best of our knowledge, this is the first demonstration of 2D pattern transfer of densely packed anisotropic features with a critical dimension below 5 nm. The techniques developed and demonstrated in this work could impact several sectors by enabling single-digit nanofabrication of various morphologies for use in integrated circuits, memory devices, optoelectronics, metasurfaces, and quantum devices. For example, the NC colloidal lithography approach could be used to fabricate uniform, high-density arrays of structures that are small enough to isolate single defects in doped materials, which would provide a significant step forward for developing quantum electronic and photonic devices.

Control over the material, shape, size, and dispersity of the NC building blocks offers flexibility in the exploration of nanoscale patterning and pattern transfer. This fabrication platform offers the opportunity to leverage the extensive library of NCs to generate arbitrarily complex patterns. Rare-earth halides and chalcogenides represent promising candidates due to their anisotropic morphologies[66,73,74] and potential for high etch selectivity. There is also opportunity to explore using different ligand sizes to tune the NC spacing.[62] Furthermore, this pattern transfer approach could be extended to any substrate material given a sufficient etch chemistry. This could include metals, less traditional semiconductors, magnetic materials, dielectric materials, amorphous materials, and quantum materials like doped diamond or 2D materials. Our fabrication strategy enables broader access to patterning at the deep nanoscale by implementing innovative processes into well-established fabrication methods while minimizing process complexity.

■ ASSOCIATED CONTENT

Supporting Information

The Supporting Information is available free of charge at https://pubs.acs.org/doi/10.1021/acs.nanolett.1c04761.

Additional information on experimental methods, characterization of the GdF_3 nanocrystals, further characterization of pattern transfer, and additional figures as referenced in the text (PDF)

https://doi.org/10.1021/acs.nanolett.1c04761
Nano Lett. 2022, 22, 1992−2000

AUTHOR INFORMATION

Corresponding Authors

Christopher B. Murray − *Department of Materials Science and Engineering and Department of Chemistry, University of Pennsylvania, Philadelphia, Pennsylvania 19104, United States*; Email: cbmurray@sas.upenn.edu

Cherie R. Kagan − *Department of Materials Science and Engineering, Department of Chemistry, and Department of Electrical and Systems Engineering, University of Pennsylvania, Philadelphia, Pennsylvania 19104, United States*; orcid.org/0000-0001-6540-2009; Email: kagan@seas.upenn.edu

Authors

Austin W. Keller − *Department of Materials Science and Engineering, University of Pennsylvania, Philadelphia, Pennsylvania 19104, United States*; orcid.org/0000-0003-1288-7027

Emanuele Marino − *Department of Chemistry, University of Pennsylvania, Philadelphia, Pennsylvania 19104, United States*; orcid.org/0000-0002-0793-9796

Di An − *Department of Chemistry, University of Pennsylvania, Philadelphia, Pennsylvania 19104, United States;* Present Address: Huawei Technologies, Pudong New District, Shanghai 200122, China

Steven J. Neuhaus − *Department of Materials Science and Engineering, University of Pennsylvania, Philadelphia, Pennsylvania 19104, United States*; orcid.org/0000-0002-6754-1165

Katherine C. Elbert − *Department of Chemistry, University of Pennsylvania, Philadelphia, Pennsylvania 19104, United States;* Present Address: Dow Chemical Company, Collegeville, Pennsylvania 19426, United States.; orcid.org/0000-0001-9019-1506

Complete contact information is available at: https://pubs.acs.org/10.1021/acs.nanolett.1c04761

Notes

Aspects of this work have been included in a provisional U.S. patent filing.

The authors declare no competing financial interest.

ACKNOWLEDGMENTS

Primary support for this work was provided by the Semiconductor Research Corporation (SRC) under the Nanomanufacturing Materials and Processes (NMP) thrust under Task 2797.001, which supported NC synthesis, microscopy, and use of clean room facilities. Additional support for electron microscopy and spectroscopy characterization was provided by the NSF MRSEC program under Award No. DMR-1720530. SAXS characterization was supported by the Office of Naval Research (ONR) Multidisciplinary University Research Initiative (MURI) Award ONR N00014-18-1-2497. Dendrimer synthesis was supported by the NSF Graduate Research Fellowship Program under Grant No. DGE-1321851. This work was carried out in part at the Singh Center for Nanotechnology, which is supported by the NSF National Nanotechnology Coordinated Infrastructure (NNCI) Program under grant NNCI-2025608.

REFERENCES

(1) Wu, B.; Kumar, A. Extreme Ultraviolet Lithography: A Review. *J. Vac. Sci. Technol. B Microelectron. Nanom. Struct. Process. Meas. Phenom.* **2007**, *25*, 1743.

(2) Suzuki, J.; Furukawa, T.; Miyata, H.; Shiratani, M.; Naruoka, T.; Maruyama, K.; Nakagawa, H.; Nagai, T. Novel EUV Photoresist for Sub-7 nm Node. *J. Photopolym. Sci. Technol.* **2017**, *30* (6), 671−674.

(3) Zahlten, C.; Gräupner, P.; van Schoot, J.; Kuerz, P.; Stoeldraijer, J.; Kaiser, W. High-NA EUV Lithography: Pushing the Limits. *Proceedings of SPIE* **2019**, 43.

(4) Yoon, G.; Tanaka, T.; Zentgraf, T.; Rho, J. Recent Progress on Metasurfaces: Applications and Fabrication. *J. Phys. D. Appl. Phys.* **2021**, *54*, 383002.

(5) Shi, H.; Zhu, X.; Zhang, S.; Wen, G.; Zheng, M.; Duan, H. Plasmonic Metal Nanostructures with Extremely Small Features: New Effects, Fabrication and Applications. *Nanoscale Adv.* **2021**, *3*, 4349−4369.

(6) Zheng, Z.; Zu, X.; Zhang, Y.; Zhou, W. Rational Design of Type-II Nano-Heterojunctions for Nanoscale Optoelectronics. *Materials Today Physics.* **2020**, *15*, 100262.

(7) Baghdadi, R.; Arpaia, R.; Charpentier, S.; Golubev, D.; Bauch, T.; Lombardi, F. Fabricating Nanogaps in YBa2Cu3 O7-δ for Hybrid Proximity-Based Josephson Junctions. *Phys. Rev. Appl.* **2015**, *4*, 014022.

(8) Regan, B.; Trycz, A.; Fröch, J. E.; Schaeper, O. C.; Kim, S.; Aharonovich, I. Nanofabrication of High Q_i Transferable Diamond Resonators. *Nanoscale* **2021**, *13*, 8848−8854.

(9) Kagan, C. R.; Bassett, L. C.; Murray, C. B.; Thompson, S. M. Colloidal Quantum Dots as Platforms for Quantum Information Science. *Chem. Rev.* **2021**, *121*, 3186−3233.

(10) Wood, O. R. EUVL: Challenges to Manufacturing Insertion. *J. Photopolym. Sci. Technol.* **2017**, *30* (5), 599−604.

(11) Levinson, H. J.; Brunner, T. A. Current Challenges and Opportunities for EUV Lithography. *Proceedings of SPIE* **2018**, 2.

(12) Baglin, J. E. E. Ion Beam Nanoscale Fabrication and Lithography - A Review. *Appl. Surf. Sci.* **2012**, *258*, 4103−4111.

(13) Stanford, M. G.; Lewis, B. B.; Mahady, K.; Fowlkes, J. D.; Rack, P. D. Review Article: Advanced Nanoscale Patterning and Material Synthesis with Gas Field Helium and Neon Ion Beams. *J. Vac. Sci. Technol. B, Nanotechnol. Microelectron. Mater. Process. Meas. Phenom.* **2017**, *35* (3), 030802.

(14) Lewis, S. M.; Hunt, M. S.; Derose, G. A.; Alty, H. R.; Li, J.; Wertheim, A.; De Rose, L.; Timco, G. A.; Scherer, A.; Yeates, S. G.; Winpenny, R. E. P. Plasma-Etched Pattern Transfer of Sub-10 nm Structures Using a Metal-Organic Resist and Helium Ion Beam Lithography. *Nano Lett.* **2019**, *19*, 6043−6048.

(15) He, S.; Tian, R.; Wu, W.; Li, W. Di; Wang, D. Helium-Ion-Beam Nanofabrication: Extreme Processes and Applications. *Int. J. Extrem. Manuf.* **2021**, *3*, 012001.

(16) Hu, W.; Sarveswaran, K.; Lieberman, M.; Bernstein, G. H. Sub-10 nm Electron Beam Lithography Using Cold Development of Poly(Methylmethacrylate). *J. Vac. Sci. Technol. B Microelectron. Nanom. Struct. Process. Meas. Phenom* **2004**, *22*, 1711−1716.

(17) Chen, Y. Nanofabrication by Electron Beam Lithography and Its Applications: A Review. *Microelectron. Eng.* **2015**, *135*, 57−72.

(18) Manfrinato, V. R.; Camino, F. E.; Stein, A.; Zhang, L.; Lu, M.; Stach, E. A.; Black, C. T. Patterning Si at the 1 nm Length Scale with Aberration-Corrected Electron-Beam Lithography: Tuning of Plasmonic Properties by Design. *Adv. Funct. Mater.* **2019**, *29*, 1903429.

(19) Ryu Cho, Y. K.; Rawlings, C. D.; Wolf, H.; Spieser, M.; Bisig, S.; Reidt, S.; Sousa, M.; Khanal, S. R.; Jacobs, T. D. B.; Knoll, A. W. Sub-10 Nanometer Feature Size in Silicon Using Thermal Scanning Probe Lithography. *ACS Nano* **2017**, *11*, 11890−11897.

(20) Howell, S. T.; Grushina, A.; Holzner, F.; Brugger, J. Thermal Scanning Probe Lithography—a Review. *Microsystems Nanoeng.* **2020**, *6*, 21.

(21) Kaestner, M.; Rangelow, I. W. Scanning Probe Lithography on Calixarene towards Single-Digit Nanometer Fabrication. *Int. J. Extrem. Manuf.* **2020**, *2*, 032005.

(22) Schift, H. Nanoimprint Lithography: An Old Story in Modern Times? A Review. *J. Vac. Sci. Technol. B Microelectron. Nanom. Struct.* **2008**, *26* (2), 458−480.
(23) Kwon, B.; Kim, J. H. Importance of Molds for Nanoimprint Lithography: Hard, Soft, and Hybrid Molds. *J. Nanosci.* **2016**, *2016*, 6571297.
(24) Oh, D. K.; Lee, T.; Ko, B.; Badloe, T.; Ok, J. G.; Rho, J. Nanoimprint Lithography for High-Throughput Fabrication of Metasurfaces. *Frontiers of Optoelectronics* **2021**, *14*, 229−251.
(25) Spende, A.; Sobel, N.; Lukas, M.; Zierold, R.; Riedl, J. C.; Gura, L.; Schubert, I.; Moreno, J. M. M.; Nielsch, K.; Stühn, B.; Hess, C.; Trautmann, C.; Toimil-Molares, M. E. TiO2, SiO2, and Al2O3 Coated Nanopores and Nanotubes Produced by ALD in Etched Ion-Track Membranes for Transport Measurements. *Nanotechnology* **2015**, *26*, 335301.
(26) Walavalkar, S. S.; Hofmann, C. E.; Homyk, A. P.; Henry, M. D.; Atwater, H. A.; Scherer, A. Tunable Visible and Near-IR Emission from Sub-10 nm Etched Single-Crystal Si Nanopillars. *Nano Lett.* **2010**, *10*, 4423−4428.
(27) Oh, D. K.; Jeong, H.; Kim, J.; Kim, Y.; Kim, I.; Ok, J. G.; Rho, J. Top-down Nanofabrication Approaches toward Single-Digit-Nanometer Scale Structures. *J. Mech. Sci. Technol.* **2021**, *35* (3), 837−859.
(28) Chou, S. Y.; Krauss, P. R.; et al. Sub-10 nm Imprint Lithography and Applications. *J. Vac. Sci. Technol. B Microelectron. Nanom. Struct. Process. Meas. Phenom.* **1997**, *15*, 2897−2904.
(29) Austin, M. D.; Ge, H.; Wu, W.; Li, M.; Yu, Z.; Wasserman, D.; Lyon, S. A.; Chou, S. Y. Fabrication of 5 nm Linewidth and 14 nm Pitch Features by Nanoimprint Lithography. *Appl. Phys. Lett.* **2004**, *84* (26), 5299−5301.
(30) Pina-Hernandez, C.; Fu, P. F.; Guo, L. J. Ultrasmall Structure Fabrication via a Facile Size Modification of Nanoimprinted Functional Silsesquioxane Features. *ACS Nano* **2011**, *5* (2), 923−931.
(31) Pi, S.; Lin, P.; Xia, Q. Fabrication of Sub-10 nm Metal Nanowire Arrays with Sub-1 nm Critical Dimension Control. *Nanotechnology* **2016**, *27*, 464004.
(32) Schvartzman, M.; Wind, S. J. Robust Pattern Transfer of Nanoimprinted Features for Sub-5 nm Fabrication. *Nano Lett.* **2009**, *9* (10), 3629−3634.
(33) Mirza, M. M.; Zhou, H.; Velha, P.; Li, X.; Docherty, K. E.; Samarelli, A.; Ternent, G.; Paul, D. J. Nanofabrication of High Aspect Ratio (∼50:1) Sub-10 nm Silicon Nanowires Using Inductively Coupled Plasma Etching. *J. Vac. Sci. Technol. B, Nanotechnol. Microelectron. Mater. Process. Meas. Phenom* **2012**, *30*, 06FF02.
(34) Peroz, C.; Dhuey, S.; Cornet, M.; Vogler, M.; Olynick, D.; Cabrini, S. Single Digit Nanofabrication by Step-and-Repeat Nanoimprint Lithography. *Nanotechnology* **2012**, *23*, 015305.
(35) Cheng, J. Y.; Mayes, A. M.; Ross, C. A. Nanostructure Engineering by Templated Self-Assembly of Block Copolymers. *Nat. Mater.* **2004**, *3* (11), 823−828.
(36) Stoykovich, M. P.; Kang, H.; Daoulas, K. C.; Liu, G.; Liu, C. C.; De Pablo, J. J.; Müller, M.; Nealey, P. F. Directed Self-Assembly of Block Copolymers for Nanolithography: Fabrication of Isolated Features and Essential Integrated Circuit Geometries. *ACS Nano* **2007**, *1* (3), 168−175.
(37) Hu, H.; Gopinadhan, M.; Osuji, C. O. Directed Self-Assembly of Block Copolymers: A Tutorial Review of Strategies for Enabling Nanotechnology with Soft Matter. *Soft Matter* **2014**, *10*, 3867−3889.
(38) Maher, M. J.; Mori, K.; Sirard, S. M.; Dinhobl, A. M.; Bates, C. M.; Gurer, E.; Blachut, G.; Lane, A. P.; Durand, W. J.; Carlson, M. C.; Strahan, J. R.; Ellison, C. J.; Willson, C. G. Pattern Transfer of Sub-10 nm Features via Tin-Containing Block Copolymers. *ACS Macro Lett.* **2016**, *5*, 391−395.
(39) Lane, A. P.; Yang, X.; Maher, M. J.; Blachut, G.; Asano, Y.; Someya, Y.; Mallavarapu, A.; Sirard, S. M.; Ellison, C. J.; Willson, C. G. Directed Self-Assembly and Pattern Transfer of Five Nanometer Block Copolymer Lamellae. *ACS Nano* **2017**, *11*, 7656−7665.
(40) Pang, Y.; Jin, X.; Huang, G.; Wan, L.; Ji, S. Directed Self-Assembly of Styrene-Methyl Acrylate Block Copolymers with Sub-7 nm Features via Thermal Annealing. *Macromolecules* **2019**, *52*, 2987−2994.
(41) Gusmão Cacho, M. G.; Pimenta-Barros, P.; Argoud, M.; Navarro, C.; Sakavuyi, K.; Tiron, R.; Possémé, N. Etching of Sub-10 nm Half-Pitch High Chi Block Copolymers for Directed Self-Assembly (DSA) Application. *Microelectron. Eng.* **2020**, *230*, 111369.
(42) Chen, Y.; Xiong, S. Directed Self-Assembly of Block Copolymers for Sub-10 nm Fabrication. *International Journal of Extreme Manufacturing* **2020**, *2* (3), 032006.
(43) Park, S.-M.; Liang, X.; Harteneck, B. D.; Pick, T. E.; Hiroshiba, N.; Wu, Y.; Helms, B. A.; Olynick, D. L. Sub-10 nm Nanofabrication via Nanoimprint Directed Self-Assembly of Block Copolymers. *ACS Nano* **2011**, *5* (11), 8523−8531.
(44) Li, J.; Zhou, C.; Chen, X.; Rincon Delgadillo, P. A.; Nealey, P. F. Orientation Control of High-χ Triblock Copolymer for Sub-10 nm Patterning Using Fluorine-Containing Polymeric Additives. *J. Micro/Nanolithography, MEMS, MOEMS* **2019**, *18* (3), 035501.
(45) Ruiz, R.; Kang, H.; Detcheverry, F. A.; Dobisz, E.; Kercher, D. S.; Albrecht, T. R.; De Pablo, J. J.; Nealey, P. F. Density Multiplication and Improved Lithography by Directed Block Copolymer Assembly. *Science* **2008**, *321* (5891), 936−939.
(46) Xiong, S.; Wan, L.; Ishida, Y.; Chapuis, Y. A.; Craig, G. S. W.; Ruiz, R.; Nealey, P. F. Directed Self-Assembly of Triblock Copolymer on Chemical Patterns for Sub-10 nm Nanofabrication via Solvent Annealing. *ACS Nano* **2016**, *10* (8), 7855−7865.
(47) Ji, S.; Wan, L.; Liu, C.-C.; Nealey, P. F. Directed Self-Assembly of Block Copolymers on Chemical Patterns: A Platform for Nanofabrication. *Prog. Polym. Sci.* **2016**, *5455*, 76−127.
(48) Tseng, Y. C.; Peng, Q.; Ocola, L. E.; Elam, J. W.; Darling, S. B. Enhanced Block Copolymer Lithography Using Sequential Infiltration Synthesis. *J. Phys. Chem. C* **2011**, *115*, 17725−17729.
(49) Peng, Q.; Tseng, Y. C.; Darling, S. B.; Elam, J. W. A Route to Nanoscopic Materials via Sequential Infiltration Synthesis on Block Copolymer Templates. *ACS Nano* **2011**, *5* (6), 4600−4606.
(50) Cara, E.; Murataj, I.; Milano, G.; De Leo, N.; Boarino, L.; Lupi, F. F. Recent Advances in Sequential Infiltration Synthesis (SIS) of Block Copolymers (BCPs). *Nanomaterials* **2021**, *11* (4), 994.
(51) Kuo, C. W.; Shiu, J. Y.; Chen, P.; Somorjai, G. A. Fabrication of Size-Tunable Large-Area Periodic Silicon Nanopillar Arrays with Sub-10-nm Resolution. *J. Physi. Chem. B* **2003**, *107* (37), 9950−9953.
(52) Yang, S. M.; Jang, S. G.; Choi, D. G.; Kim, S.; Yu, H. K. Nanomachining by Colloidal Lithography. *Small* **2006**, *2* (4), 458−475.
(53) Zhang, J.; Li, Y.; Zhang, X.; Yang, B. Colloidal Self-Assembly Meets Nanofabrication: From Two-Dimensional Colloidal Crystals to Nanostructure Arrays. *Adv. Mater.* **2010**, *22* (38), 4249−4269.
(54) Ye, X.; Qi, L. Two-Dimensionally Patterned Nanostructures Based on Monolayer Colloidal Crystals: Controllable Fabrication, Assembly, and Applications. *Nano Today* **2011**, *6* (6), 608−631.
(55) Lotito, V.; Zambelli, T. Self-Assembly and Nanosphere Lithography for Large-Area Plasmonic Patterns on Graphene. *J. Colloid Interface Sci.* **2015**, *447*, 202−210.
(56) Ai, B.; Möhwald, H.; Wang, D.; Zhang, G. Advanced Colloidal Lithography Beyond Surface Patterning. *Advanced Materials Interfaces* **2017**, *4* (1), 1600271.
(57) Liu, J.; Zhang, X.; Li, W.; Jiang, C.; Wang, Z.; Xiao, X. Recent Progress in Periodic Patterning Fabricated by Self-Assembly of Colloidal Spheres for Optical Applications. *Science China Materials* **2020**, *63*, 1418−1437.
(58) Rey, M.; Wendisch, F. J.; Aaron Goerlitzer, E. S.; Julia Tang, J. S.; Bader, R. S.; Bourret, G. R.; Vogel, N. Anisotropic Silicon Nanowire Arrays Fabricated by Colloidal Lithography. *Nanoscale Adv.* **2021**, *3* (12), 3634−3642.
(59) Hogg, C. R.; Majetich, S. A.; Bain, J. A. Investigating Pattern Transfer in the Small-Gap Regime Using Electron-Beam Stabilized Nanoparticle Array Etch Masks. *IEEE Trans. Magn.* **2010**, *46* (6), 2307−2310.

https://doi.org/10.1021/acs.nanolett.1c04761
Nano Lett. 2022, 22, 1992−2000

(60) Wen, T.; Booth, R. A.; Majetich, S. A. Ten-Nanometer Dense Hole Arrays Generated by Nanoparticle Lithography. *Nano Lett.* **2012**, *12* (11), 5873−5878.
(61) Hogg, C. R.; Picard, Y. N.; Narasimhan, A.; Bain, J. A.; Majetich, S. A. Pattern Transfer with Stabilized Nanoparticle Etch Masks. *Nanotechnology* **2013**, *24*, 085303.
(62) Jishkariani, D.; Diroll, B. T.; Cargnello, M.; Klein, D. R.; Hough, L. A.; Murray, C. B.; Donnio, B. Dendron-Mediated Engineering of Interparticle Separation and Self-Assembly in Dendronized Gold Nanoparticles Superlattices. *J. Am. Chem. Soc.* **2015**, *137* (33), 10728−10734.
(63) Hatzor, A.; Weiss, P. S. Molecular Rulers for Scaling Down Nanostructures. *Science* **2001**, *291*, 1019−1020.
(64) Santhanam, V.; Liu, J.; Agarwal, R.; Andres, R. P. Self-Assembly of Uniform Monolayer Arrays of Nanoparticles. *Langmuir* **2003**, *19*, 7881−7887.
(65) Dong, A.; Chen, J.; Vora, P. M.; Kikkawa, J. M.; Murray, C. B. Binary Nanocrystal Superlattice Membranes Self-Assembled at the Liquid-Air Interface. *Nature* **2010**, *466* (7305), 474−477.
(66) Ye, X.; Collins, J. E.; Kang, Y.; Chen, J.; Chen, D. T. N.; Yodh, A. G.; Murray, C. B. Morphologically Controlled Synthesis of Colloidal Upconversion Nanophosphors and Their Shape-Directed Self-Assembly. *Proc. Natl. Acad. Sci. U.S.A.* **2010**, *107* (52), 22430−22435.
(67) Elbert, K. C.; Vo, T.; Krook, N. M.; Zygmunt, W.; Park, J.; Yager, K. G.; Composto, R. J.; Glotzer, S. C.; Murray, C. B. Dendrimer Ligand Directed Nanoplate Assembly. *ACS Nano* **2019**, *13*, 14241−14251.
(68) *Plasma Etching: An Introduction*; Manos, D. M., Flamm, D. L., Eds.; Academic Press Inc.: London, 1989.
(69) Nojiri, K. *Dry Etching Technology for Semiconductors*; Springer International Publishing, 2015.
(70) Chen, Y.; Shu, Z.; Zhang, S.; Zeng, P.; Liang, H.; Zheng, M.; Duan, H. Sub-10 nm Fabrication: Methods and Applications. *Int. J. Extrem. Manuf.* **2021**, *3* (3), 032002.
(71) Haase, M.; Schäfer, H. Upconverting Nanoparticles. *Angew. Chemie - Int. Ed.* **2011**, *50*, 5808−5829.
(72) Najmr, S.; Lu, T.; Keller, A. W.; Zhang, M.; Lee, J. D.; Makvandi, M.; Pryma, D. A.; Kagan, C. R.; Murray, C. B. Preparation of Silica Coated and 90Y-Radiolabeled β-NaYF4 Upconverting Nanophosphors for Multimodal Tracing. *Nano Futur.* **2018**, *2*, 025002.
(73) Sun, X.; Zhang, Y. W.; Du, Y. P.; Yan, Z. G.; Si, R.; You, L. P.; Yan, C. H. From Trifluoroacetate Complex Precursors to Monodisperse Rare-Earth Fluoride and Oxyfluoride Nanocrystals with Diverse Shapes through Controlled Fluorination in Solution Phase. *Chem. - A Eur. J.* **2007**, *13* (8), 2320−2332.
(74) Gouget, G.; Pellerin, M.; Al Rahal Al Orabi, R.; Pautrot-D'Alençon, L.; Le Mercier, T.; Murray, C. B. Rare-Earth Sulfide Nanocrystals from Wet Colloidal Synthesis: Tunable Compositions, Size-Dependent Light Absorption, and Sensitized Rare-Earth Luminescence. *J. Am. Chem. Soc.* **2021**, *143* (9), 3300−3305.

https://doi.org/10.1021/acs.nanolett.1c04761
Nano Lett. 2022, 22, 1992−2000